



# An ultra-broadband terahertz absorber at high terahertz frequency

Tong Li<sup>1</sup> · Hang Chen<sup>1</sup> · Fengqiang Zhang<sup>3</sup> · Jia Zhang<sup>1,2</sup> · Zhenlong Wang<sup>1,2</sup>

Received: 22 December 2021 / Accepted: 22 August 2022 / Published online: 22 October 2022  
© The Author(s), under exclusive licence to Springer Science+Business Media, LLC, part of Springer Nature 2022

## Abstract

Broadband absorber at high terahertz frequency is highly required for applications in imaging, detecting, electromagnetic stealth. Although intensive investigations of the broadband absorber have been taken, the challenges still exist both in design and fabrication of an ultra-broadband absorber at high frequency. Herein, a three-layered structure metamaterial has been designed to realize an ultra-broadband terahertz absorber covering 3.94–9.98 THz (6.04 THz) at the absorption above 80%, and the absorption bandwidth can be increased to 7.64 THz (2.34–9.98 THz) by rotating the absorber. Upon on the simulations, the proposed absorber exhibits insensitive to the TM and TE polarization, it means the absorption effect is almost consistent in different polarization modes, the proposed absorber is significant in the practical application. Nevertheless, the absorption bandwidth reduces a little bit to 5.05 THz (absorption > 60%) as  $\beta$  increases to 45°.

**Keywords** Terahertz · Broadband absorber · Metamaterials

## 1 Introduction

Terahertz wave is a kind of electromagnetic wave with a frequency range of 0.1–10 THz (Siegel 2002; Yen et al. 2004; Song et al. 2018), which has many unique advantages of strong penetrability, high resolution and low photon energy (Jiang et al. 2018; Pitchappa et al. 2016; Song et al. 2020). It has great potential in imaging, nondestructive detection, spectrum analysis (Chen et al. 2020a, 2020b; Abramov et al. 2021). The discovery of electromagnetic metamaterials has provided a novel approach for preparation of terahertz absorbing material. Since the first experimental demonstration of a near-perfect microwave

---

✉ Jia Zhang  
zhangjia@hit.edu.cn

✉ Zhenlong Wang  
wangzl@hit.edu.cn

<sup>1</sup> School of Mechatronics Engineering, Harbin Institute of Technology, Harbin 150001, China

<sup>2</sup> Key Laboratory of Microsystems and Microstructures Manufacturing, Ministry of Education, Harbin Institute of Technology, Harbin 150080, China

<sup>3</sup> School of Mechatronics Engineering and Automation, Harbin Institute of Technology, Shenzhen 518055, China

metamaterial absorber has been conducted (Landy et al. 2008), the metamaterial terahertz absorber has received extensive attentions and researches (Wu et al. 2021; Biabanifard et al. 2020; Bai et al. 2018). However, most attempts are focused on the single absorption frequencies or narrow-band absorption of absorber (Ma et al. 2011; Xu et al. 2020; Huang et al. 2020; Verma et al. 2020; Wang et al. 2020). Actually, the broadband absorber can absorb more electromagnetic waves, it is more important in the fields, such as electromagnetic stealth, terahertz imaging and sensing. For electromagnetic stealth, the broadband absorber can absorb more terahertz wave at different frequency, it means less electromagnetic waves were reflected, finally less reflected electromagnetic waves could be accepted by radar, it's good for evading the search of radar. For terahertz imaging, the reflected THZ waves would be converted to image signal, and broadband absorber can absorb more reflected THZ waves at different frequency, it's good of improving the image accuracy. For terahertz sensing, broadband absorber can absorb more THZ waves which contains more information, it's good of improving the performance of THZ sensor.

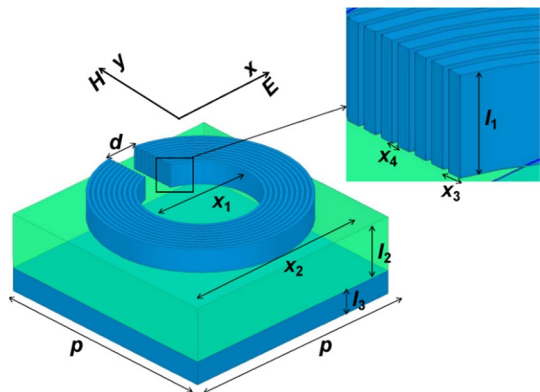
In the last decade, many attempts of preparation of broadband absorbers have been made, however, the absorption bands are almost in the low terahertz frequency (0.1–5 THz) (Huang et al. 2018; Zhu et al. 2019; Wang et al. 2014). There is still challenges for designing ultra-broadband absorber at the high terahertz frequency (Liu et al. 2019; Daraei et al. 2020; Mohamadreza et al. 2020).

In this letter, an ultra-broadband terahertz absorber was proposed, which is a metamaterial with a three-layered structure. The absorption of THZ absorber can be above 80% in the high frequency of 3.94–9.98 THz, and almost above 60% at the entire terahertz frequency band. The special designed ten nested aluminum rings with an opening structure will response for such an ultra-broadband absorption. Significantly, the proposed absorber exhibits insensitive to the TM and TE polarization no matter what kinds of incident angles are applied.

## 2 Structure and design

The proposed broadband absorber is a kind of periodic metamaterials, and the cell is schematically illustrated in Fig. 1. It contains three layers: a metallic bottom layer, another metallic top layer and a dielectric middle layer. The proposed metamaterial absorber is represented as “NROS” (nested rings with an opening structure) absorber.

**Fig. 1** 3D model of the cell of the proposed absorber. Enlarged view shows the nested rings of top layer. All structural parameters are marked with black symbol



Specifically, the top layer is consisted of ten nested rings with an opening structure. The diameter of the innermost and outmost circle is represented as  $x_1$  and  $x_2$ , while the width of each circle and inter distance of adjacent circles is recorded as  $x_3$  and  $x_4$ , respectively. The width of opening structure is  $d$ , and the period of the unit cell both in  $x$  and  $y$  directions is  $p$ . The thickness of each layer from top to down is defined as  $l_1$ ,  $l_2$  and  $l_3$ , respectively. Based on the systematic simulations, the absorption can achieve maximum value when both the relative permittivity ( $\epsilon_1$ ) and permeability ( $\mu_1$ ) of metallic layer are about 1. Meanwhile, the  $\epsilon_2$  and  $\mu_2$  of middle dielectric layer should be about 3.5 and 1, respectively. Therefore, the aluminum metal is chosen for both of top and bottom layer, while polyethylene is selected to the middle dielectric layer with  $\epsilon_2=3.5$  and  $\mu_2=1$ , respectively. All the design parameters are shown in Table 1.

The simulations of the periodic structure are carried out by employing finite difference time domain method based on “ANSYS Electronics 2017”. Absorption can be calculated by  $A(\omega)=1-R(\omega)-T(\omega)$ ,  $R(\omega)$  is reflectivity,  $T(\omega)$  is transmissivity.  $S_{11}$  is reflection coefficient,  $S_{21}$  is transmission coefficient,  $R(\omega)=|S_{11}|^2$ ,  $T(\omega)=|S_{21}|^2$ . According to the matrix transmission principle, the transmission matrix of electromagnetic wave in metamaterials can be calculated as:

$$T = \begin{pmatrix} \cos(nkh) & -\frac{z}{k} \sin(nkh) \\ \frac{k}{z} \sin(nkh) & \cos(nkh) \end{pmatrix} \tag{1}$$

In the Eq. 1,  $n$  is refractive index of uniform tablet,  $k$  is wave vector of incident wave,  $h$  is thickness of uniform tablet,  $z$  is equivalent impedance of medium plate. The structure size of metamaterials is much smaller than the working wavelength, the metamaterials can be consider as homogeneous materials.  $S_{11}$  and  $S_{21}$  can be calculated as:

$$S_{11} = \frac{i}{2} \left( \frac{1}{z} - z \right) \sin(nkh) \tag{2}$$

$$S_{21} = \frac{1}{\cos(nkh) - \frac{i}{2} \left( z + \frac{1}{z} \right) \sin(nkh)} \tag{3}$$

Equation 4 shows the relation of refractive index ( $n$ ), impedance ( $z$ ), permittivity ( $\epsilon$ ), and permeability ( $\mu$ ).

$$n = \epsilon z = \frac{\mu}{z} \tag{4}$$

**Table 1** Design parameters of proposed metamaterial absorber

Layer	Structure parameters	Materials	
		Name	Physical parameters
Top layer	$d=5 \mu\text{m}$ , $x_1=14.4 \mu\text{m}$ , $x_2=26 \mu\text{m}$ , $x_3=0.4 \mu\text{m}$ , $x_4=0.2 \mu\text{m}$ , $l_1=0.02 \mu\text{m}$ $p=30 \mu\text{m}$	Aluminum	$\epsilon_1=1$ , $\mu_1=1.000021$
Dielectric layer	$l_2=7 \mu\text{m}$	Polyimide	$\epsilon_2=3.5$ , $\mu_2=1$
Bottom layer	$l_3=1 \mu\text{m}$	Aluminum	$\epsilon_1=1$ , $\mu_1=1.000021$

According to Eq. (2–4), the relation between  $S_{11}$ ,  $S_{21}$  and  $z$ ,  $n$ ,  $\epsilon$ ,  $\mu$  can be deduced (see Eq. 5–8).

$$z = \sqrt{\frac{(1 + S_{11})^2 - S_{21}^2}{(1 - S_{11})^2 - S_{21}^2}} \tag{5}$$

$$n = \frac{1}{kh} \cos^{-1} \left[ \frac{1}{2S_{21}} (1 - S_{11}^2 + S_{21}^2) \right] \tag{6}$$

$$\epsilon = \frac{1}{kh} \cos^{-1} \left[ \frac{1}{2S_{21}} (1 - S_{11}^2 + S_{21}^2) \sqrt{\frac{1 - S_{11}^2 - S_{21}^2}{(1 + S_{11})^2 - S_{21}^2}} \right] \tag{7}$$

$$\mu = \frac{1}{kh} \cos^{-1} \left[ \frac{1}{2S_{21}} (1 - S_{11}^2 + S_{21}^2) \sqrt{\frac{(1 + S_{11})^2 - S_{21}^2}{1 - S_{11}^2 - S_{21}^2}} \right] \tag{8}$$

According to impedance matching principle, when equivalent impedance ( $z$ ) is closer to the impedance of metamaterial interface with air, the reflectivity is lower. As Eq. 4 shown, we can change the impedance ( $z$ ) by controlling permittivity ( $\epsilon$ ). For the metamaterial absorber, the permittivity ( $\epsilon$ ) can be selected by controlling the size and geometry of periodic structure.

Different from the ‘‘CNR’’ (closed and nested rings) absorber, NROS absorber has an opening structure in the nested rings which makes a better absorption broadband. Figure 2(a-d) are the electric fields of CNR and NROS metamaterial absorber at their resonance frequency, the electric fields are mainly distributed in the horizontal metal line of the closed nested metal ring in the resonant state, it means the horizontal metal line of the closed nested metal ring is equivalent to inductance ( $L$ ), the vertical metal line is equivalent to capacitance ( $C$ ) (see Fig. 2(f)). Figure 2 (f) is equivalent circuit of CNR and NROS metamaterial absorber,  $R$  in the circuit is the equivalent resistance of energy loss.  $L$  and  $C$  are the equivalent inductance and capacitance of the metal patch structure. Whether NROS absorber or CNR absorber, each nested ring means a LC resonant circuit, there are 10 parallel LC resonant circuits in the equivalent circuit of CNR and NROS metamaterial absorber. When the metamaterial absorber is in perfect absorption, each LC resonance circuit can make an absorption curve, and the absorption curve is equivalent to the resonance curve, so the frequency of absorption peak is equal to the resonant frequency [see Eq. 9].

$$f = \frac{1}{T} = \frac{1}{2\pi\sqrt{LC}} \tag{9}$$

$T$  is the oscillation period of LC resonance circuits, it also can be the bandwidth of absorption. There are ten LC resonance circuits, it means there would be ten absorption curves, making ten absorption curves closer by controlling  $L$  and  $C$ , finally get an broadband absorption[see Fig. 2(e)].

Different from the CNR metamaterial absorber, there is an opening structure in the nested rings of NROS metamaterial absorber, it means in each parallel LC resonant

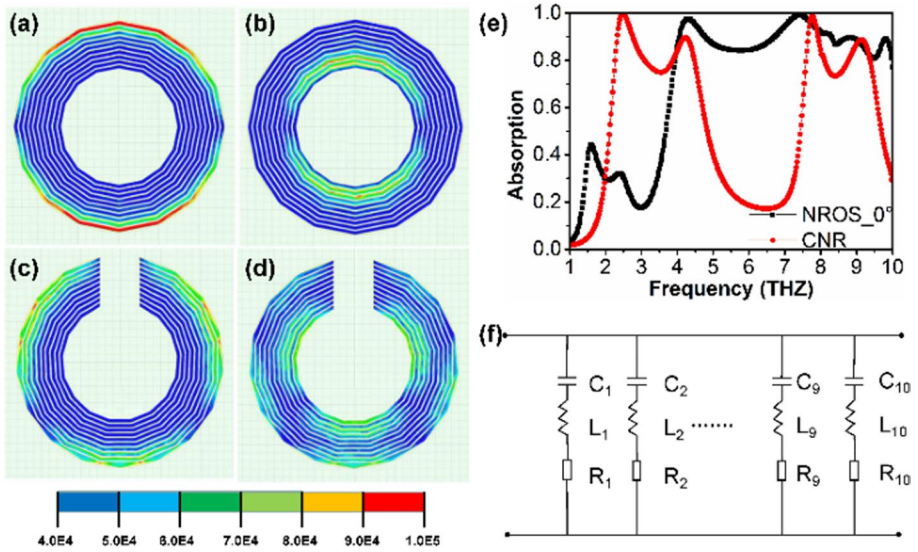


**Fig. 2** **a** The electric field distribution of the CNR metamaterial absorber at the resonance frequency 2.5 THZ. **b** The current field distribution of the CNR metamaterial absorber at the resonance frequency 4.3 THZ. **c** The current field distribution of the NROS metamaterial absorber at the resonance frequency 4.3 THZ. **d** The current field distribution of the NROS metamaterial absorber at the resonance frequency 7.2 THZ. **e** Absorption curves with optimized structural parameters of NROS absorber and CNR absorber. **f** Equivalent circuit diagram of CNR and NROS metamaterial absorber

circuit, the inductance ( $L_n$ ,  $n=1, 2, \dots, 10$ ) has been reduced [see Fig. 2(f)], while the equivalent circuit is a parallel circuit, the equivalent inductance ( $L$ ) would be increased. The equivalent inductance ( $L$ ) and equivalent capacitance ( $C$ ) could be calculated as Eq. 10–11:

$$\frac{1}{L} = \frac{1}{R_1 L_1} + \frac{1}{R_2 L_2} + \frac{1}{R_3 L_3} + \dots + \frac{1}{R_{10} L_{10}} \tag{10}$$

$$C = R_1 C_1 + R_2 C_2 + R_3 C_3 + \dots + R_{10} C_{10} \tag{11}$$

The equivalent inductance ( $L$ ) has been reduced [see Fig. 2(f)], while the period of oscillation  $T$  is in direct proportion to inductance ( $L$ ) [see Eq. 9],  $T$  of NROS absorber is longer than CNR absorber, it leads the broadband of NROS absorber is longer than it of CNR absorber [see Fig. 2(e)].

As Fig. 2(a-d) shown, the electric field of the CNR metamaterial absorber at the resonance frequency (2.5 THZ and 4.3 THZ) is stronger than which of NROS metamaterial absorber (4.3 THZ and 7.2 THZ). In LC resonance circuit, as the electric field intensity increases, the oscillation period will decrease. As Fig. 2(a-d) shown, the electric fields of the CNR metamaterial absorber at its resonance frequency are stronger than which of NROS metamaterial absorber, it means the oscillation period of the NROS metamaterial absorber is longer than which of CNR metamaterial absorber, it also proved that the broadband of NROS absorber is longer than which of CNR absorber.

### 3 Results and discussion

Following, the angle between the open structure and the positive direction of the magnetic field was defined as  $\alpha$ , which represents the angle between the positive direction of the magnetic field and the positive direction of central axis of opening structure [Fig. 3(a)]. Both parameters of  $\alpha$  and  $d$  are proven to have highly effect on the absorption feature of the absorber. As  $d$  increases from 1 to 6  $\mu\text{m}$ , the third absorption peak (arrow in Fig. 3(b)) shifts to the high frequency gradually, and resulting in decreasing of bandwidth in the 4–8 THz. Otherwise, the absorption is below 80% in the 4–8 THz as the  $d$  is set as 1  $\mu\text{m}$ , while it is below 80% in the 9–10 THz if  $d$  is set as 6  $\mu\text{m}$  [Fig. 3(b)]. As a result,  $d$  is optimized as 5  $\mu\text{m}$  in our design. Figure 3(c, d) plot absorption curves with various values of the  $\alpha$  in the range of 0–90° at a step of 10°, respectively. The curve shape exhibits two obvious stages [Fig. 3(c, d)]. As  $\alpha$  increases from 0 to 40°, the absorption gradually reduces to below 80% in 5–8 THz, but still above 60% [Fig. 3(c)]. In contrast, as  $\alpha$  increases from 50° to 90°, the absorption broadband shifts to 2–5 THz, but the absorption increases in 2.5–3.5 THz [Fig. 3(d)]. In this terahertz band, the smallest absorption is still above 70% (3.23 THz,  $\alpha=50^\circ$ ), and the absorption broadband is calculated to be 2.8 THz (2.32–5.12 THz) at absorption above 70%. Finally, two isolated absorption broadband can be achieved as  $\alpha$  set as 50°–90°, respectively, and the absorption bandwidth can be increased to 7.64THz (2.34–9.98 THz) by controlling the  $\alpha$ .

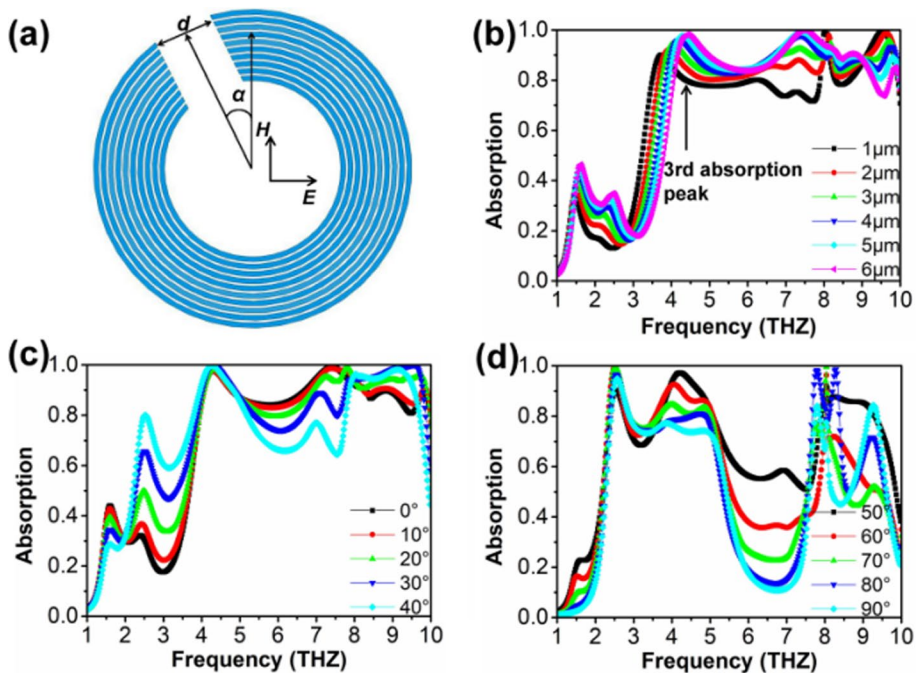


**Fig. 3** **a** Schematic diagram of the NROS absorbing structure. **b** Absorption curves of NROS absorber with various  $d$ . Absorption curves of NROS absorber as  $\alpha$  is set from 0° to 40° (**c**), and from 50° to 90° (**d**). All the absorption results are simulated by the TE polarization mode

Furthermore, the structural parameters are systematically investigated by simulations. As the thickness of top layer ( $l_1$ ) increases from 0.02 to 0.10  $\mu\text{m}$ , the absorption curves keep the similar shape but a little decrease of intensity in the 4–10 THz [Fig. 4(a)]. It indicates a little influence of the thickness of top metals. Therefore, the thickness of top metallic layer is set to 0.02  $\mu\text{m}$  in consideration of the convenience of fabrication process. For the middle dielectric layer, the absorption curves exhibit a big change at the different thicknesses ( $l_2$ ) [Fig. 4(b)]. In brief, the absorption is below 80% in 5–7 THz as  $l_2 < 7 \mu\text{m}$ , while a smaller value is found in 9–10 THz as  $l_2 > 7 \mu\text{m}$  [Fig. 4(b)]. Therefore,  $l_2$  is optimized to be 7  $\mu\text{m}$  in our design.

For the width of each ring ( $x_3$ ), it has a significant influence on the third absorption peak. As  $x_3$  increases from 0.2 to 1.0  $\mu\text{m}$ , the peak shifts to the lower frequency, which can extend absorption broadband efficiently [Fig. 4(c)]. However, there is part of absorption broadband between the third and fourth peak below 80% [Fig. 4(c)] as  $x_3 > 0.4 \mu\text{m}$ . Meanwhile, there is still a part (7.5–8.5 THz) with absorption below 80% as  $x_3 = 0.2 \mu\text{m}$ . Above all,  $x_3$  is optimized to be 0.4  $\mu\text{m}$  herein. In addition, the distance between the adjacent rings ( $x_4$ ) shows a remarkable influence on the absorption peak position and intensity. Figure 4(d) shows a down shift of the third peak as increase of  $x_4$ , leading to extend of absorption regime. Meanwhile, the absorption intensity between the third and fourth peak gradually reduces, even below 80%. For additional reason, there is much difficult and high-cost in fabrication process if narrows the adjacent distance further. Above all, the  $x_4$  was set to be 0.2  $\mu\text{m}$  finally.

For the number of rings, the absorption curves [Fig. 4(e)] show a similar behavior as those of parameter of  $x_4$ . The third peak shifts to the low frequency as increase of number from 7 to 20, thereby extending the absorption broadband efficiently. However, the absorption between the third and fourth peaks will be gradually decreased below 80% if the number is more than 10. To realize the ultra-broadband absorption and reduce the complex of fabrication process, the number of metallic rings is set to 10 in our design.

After optimization analysis, the absorption bandwidth is kept about 6.04 THz when the diameter of the innermost ( $x_1$ ) is about 14.4  $\mu\text{m}$ . Therefore, the  $x_1$  is set to be 14.4  $\mu\text{m}$  in our design. According to the optimized values of  $x_3$ ,  $x_4$  and number of rings, the diameter of the outmost circle ( $x_2$ ) is calculated to be 26  $\mu\text{m}$ . In addition, the absorption bandwidth has been kept about 6 THz when the periodicity ( $p$ ) is around 30.

After optimization of structural parameters of absorber, a broadband of 6.04 THz at high frequency of 3.94–9.98 THz is achieved at incident angle of  $0^\circ$  [Fig. 4(f) black line]. Notably, all the absorption in this regime is above 80%, with the highest and average absorption of 99.26% and 89.43%, respectively. In contrast, a controlled absorber is developed which has the same structural parameters as the NROS absorber, but with 10 closed nested rings. It is named as “CNR”. The red line in Fig. 4(f) exhibits its absorption curve. The absorption bandwidth is obtained cover two frequency regimes of 2.41 THz (from 2.23–4.64 THz) and 1.89 THz (from 7.52–9.41 THz). Nevertheless, the absorption bandwidth is narrower than that of “NROS” absorber, and the absorption is lower than 80% in most of absorption bandwidth too.

Figure 4(g) plots absorption curves in the range of 1–10 THz at TM and TE polarized incidence. Two curves are near overlapped, indicating the proposed absorber is insensitive to the TM and TE polarization. The absorption band covers from 3.94 to 9.98 THz at the absorption above 80%. This broadband of 6.04 THz at high frequency is rarely achieved before both in the simulation and experiment. Figure 4(h) depicts the absorption curves with various incident angles of  $0$ – $60^\circ$  at a step of  $15^\circ$ . Generally, the absorption curves show the similar shape with gradually decrease of intensity [Fig. 4(h)]. The largest

**Fig. 4** **a** Thickness of top metallic layer ( $l_1$ ). **b** Thickness of middle dielectric layer ( $l_2$ ). **c** Width of metallic ring ( $x_3$ ). **d** Distance of adjacent rings ( $x_4$ ). **e** Number of metallic rings. **f** Absorption curves with optimized structural parameters of NROS absorber and its controlled CNR absorber. **g** Absorption curves with different polarized incidence (TE and TM). **h** Absorption curves at polarization angles  $\varphi=0-60^\circ$  at a step of  $15^\circ$ . All the absorption results are simulated by the TE polarization mode except Fig. 4 (g)

bandwidth is calculated to be 6.23 THz at absorption above 60% achieved at  $\beta=0^\circ$ , while it reduces to its smallest value of 5.05 THz at  $\beta=45^\circ$ . The drop ratio is only 19%, suggesting the proposed NROS absorber is a terahertz polarization insensitive absorber.

To analyse the corresponding background physical mechanism to each simulation result, the electric fields of proposed absorber was shown in Fig. 5–8. Figure 5 depicts the simulated 2D patterns of the electric field distribution of the NROS and CNR absorber at different absorption peaks.

Figure 5(a-c) depict the distribution of electric field at absorption peaks of 4.3, 7.2 and 8.8 THz, respectively, when the angle  $\alpha$  is  $0^\circ$ . The position of the maximum intensity moves from outer to inner ring, and back to outer one again. Meanwhile, the maximum electric field intensity gradually decreases [Fig. 5(a-c)], and the stronger field are mainly distributed near the opening structure [Fig. 5(a-c)].

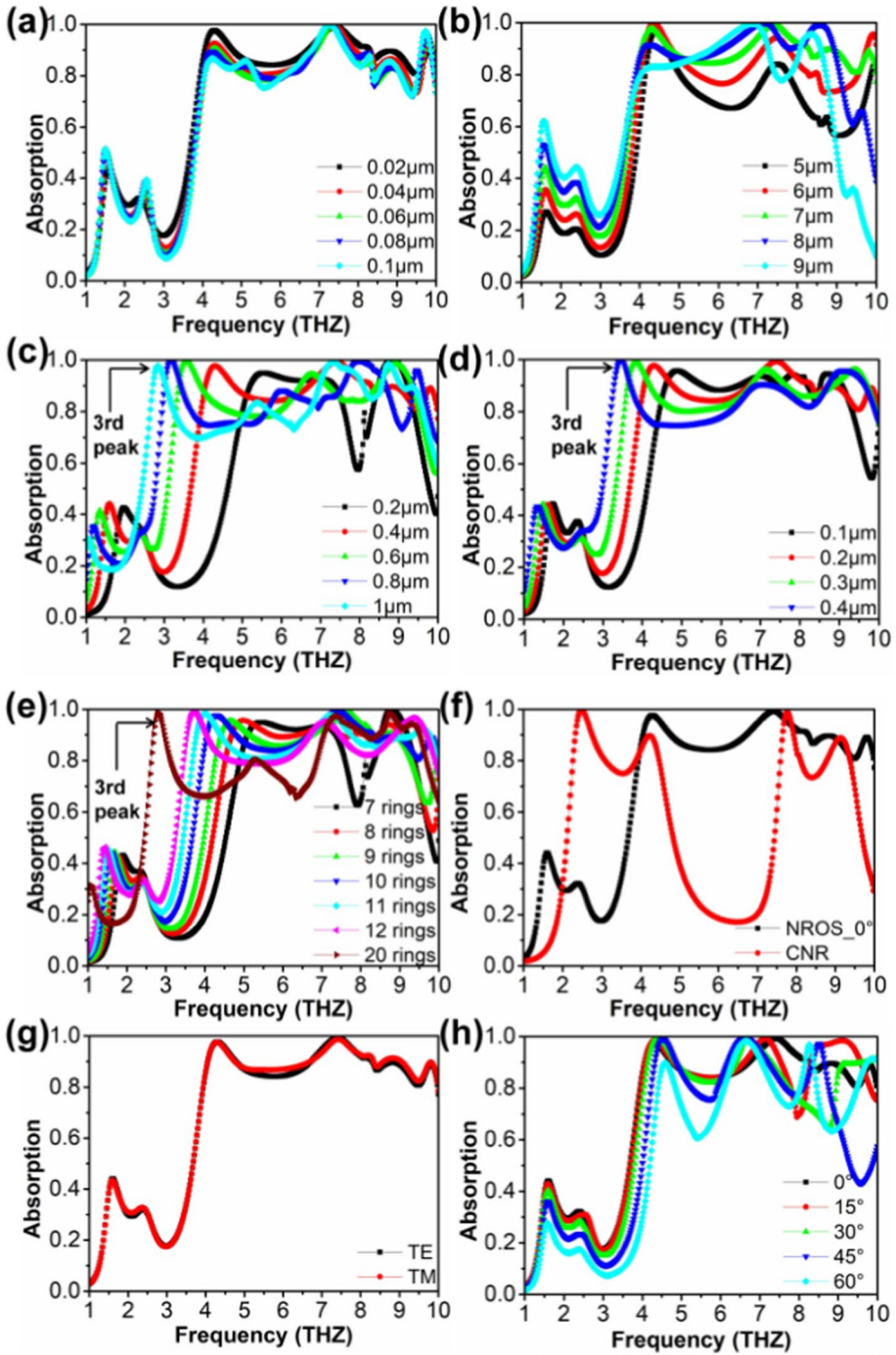
Because the horizontal metal line of the closed nested metal ring is equivalent to inductance ( $L_n$ ), the vertical metal line is equivalent to capacitance ( $C_n$ ). The opening structure of NROS absorber will make the inductance ( $L_n$ ) decreased, resulting in a decrease in equivalent inductance ( $L$ ), finally the  $f$  will increase, the absorption peak will shift right (Fig. 2e). In addition, the distribution exhibits symmetrical about the central axis of the opening structure at three absorption peaks of 2.5, 4 and 5 THz, and the stronger field are mainly distributed near the opening structure too [Fig. 5(d-f)]. As a controlled experiment, the same simulations have been carried out on the CNR absorbers to investigate the distribution of electric field. Figure 5(g-i) exhibit the field moves from outer ring to inner one, and then back to outer one again. Meanwhile, the intensity of the electric field is gradually reduced.

As  $d$  increases, the electric field intensity of proposed absorber at 3.7THz has been increased (Fig. 6a-c).

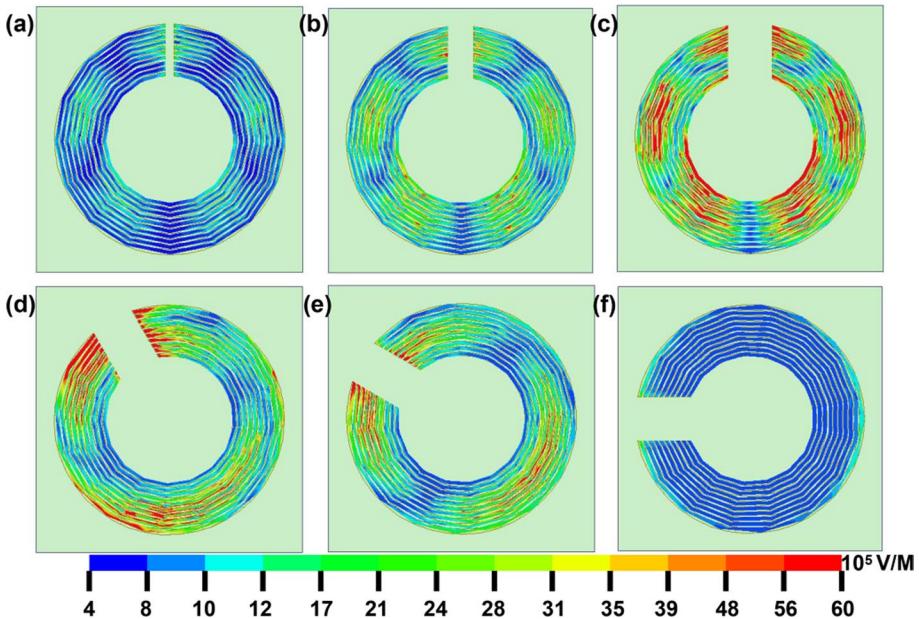
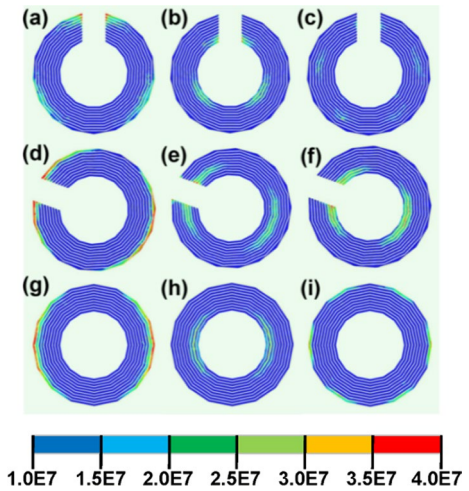
Stronger electric field intensity leads higher absorption, it agrees with the simulation results (Fig. 3b). And according to Eqs. 9 and 10, as  $d$  increases, the inductance ( $L_n$ ) ( $n=1,2,3\dots 10$ ) will decrease which leads a increase in equivalent inductance ( $L$ ), finally the resonant frequency  $f$  will be decreased, and the third absorption peak will move to the high frequency (Fig. 3b). As Fig. 6d-f shown, the electric field intensity will be decreased with  $\alpha$  increased, which makes a decrease in absorption (Fig. 3c,d).

Figure 7a-c illustrate the electric field distribution of different width of metallic ring ( $x_3$ ), absorption is positively correlated with the electric field intensity, when  $x_3$  is  $0.4\ \mu\text{m}$  the electric field intensity is strongest (Fig. 7b), it proves the red absorption curve is higher than other curves at 3.7THz (Fig. 4c), the width of metallic ring ( $x_3$ ) should be set as  $0.4\ \mu\text{m}$ . In the same way, the distance of adjacent rings ( $x_4$ ) and number of metallic rings should be set as  $0.2\ \mu\text{m}$  and 10 (Fig. 7d-f). According to Eqs. 9 and 10, the resonant frequency ( $f$ ) is negatively correlated with the equivalent inductance ( $L$ ). As  $x_3$  increases, the equivalent inductance ( $L$ ) will increase with  $L_n$  increased, which leads a decrease in resonant frequency ( $f$ ), finally the third absorption peak moves to the left (Fig. 4c). As  $x_4$  increases, the resistance ( $R_n$ ) will increase which leads the equivalent inductance ( $L$ ) increased, resulting in a decrease in the resonant frequency ( $f$ ), finally the third absorption peak moves to the left (Fig. 4d).





**Fig. 5** 2D pattern of distribution of electric field at different absorption peaks. **a–c** The absorption peaks at 4.3, 7.2, 8.8 THz at  $\alpha = 0^\circ$ , respectively. **d–f** The absorption peaks at 2.5, 4.0, 4.8 THz at  $\alpha = 70^\circ$ , respectively. **G–i** The absorption peaks at 2.4, 4.3, 7.7 THz of CNR absorber, respectively



**Fig. 6** 2D pattern of distribution of electric field of proposed absorber at 3.7THz. **a–c** The  $d$  is 1  $\mu\text{m}$ , 3  $\mu\text{m}$  and 5  $\mu\text{m}$ , respectively. **d–f** The  $\alpha$  is  $30^\circ$ ,  $60^\circ$  and  $90^\circ$ , respectively

As Fig. 7g–i shown, when the number of metallic rings is 10, the electric field intensity is strongest (Fig. 7h), it proves the blue absorption curve is higher than other curves at 3.7THz (Fig. 4e). And as the number of metallic rings increase, number of  $L_n$  and  $C_n$  will increase, which leads equivalent inductance ( $L$ ) decreased and equivalent inductance ( $C$ ) increased (see Eq. 10–11). Because the horizontal metal line of the closed nested metal ring is equivalent to inductance ( $L_n$ ), the vertical metal line is equivalent to capacitance ( $C_n$ ), and the horizontal metal line is shorter than vertical metal line, the increments of  $C$  is more

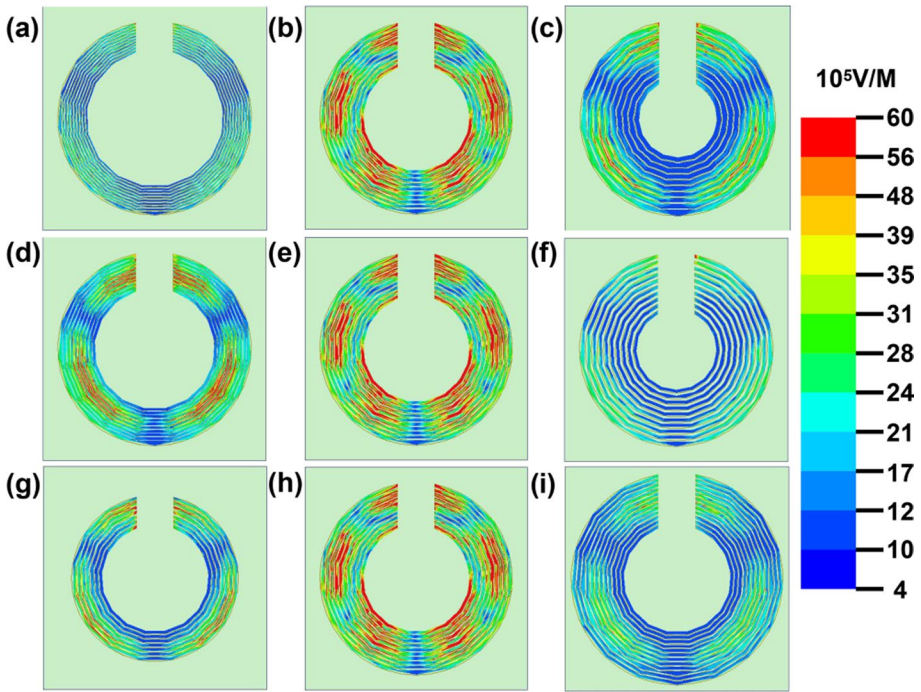


**Fig. 7** 2D pattern of distribution of electric field of proposed absorber at 3.7THz. **a–c** Width of metallic ring ( $x_3$ ) is 0.2  $\mu\text{m}$ , 0.4  $\mu\text{m}$  and 0.6  $\mu\text{m}$ , respectively. **d–f** Distance of adjacent rings ( $x_4$ ) is 0.1  $\mu\text{m}$ , 0.2  $\mu\text{m}$ , 0.3  $\mu\text{m}$ , respectively. **g–i** Number of metallic rings is 8, 10, 12, respectively

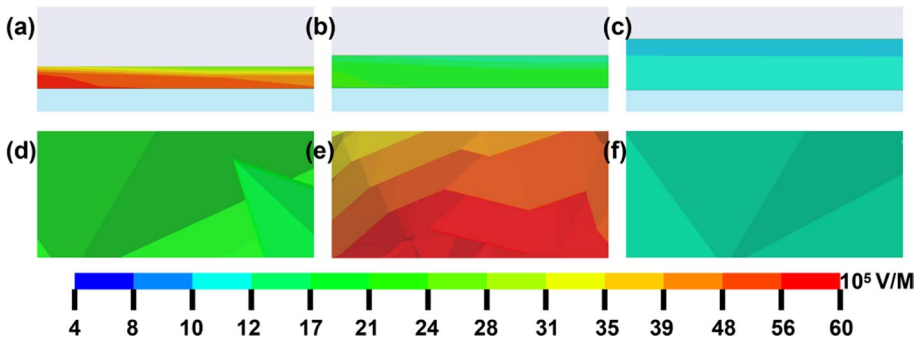


**Fig. 8** Distribution of electric field of proposed absorber at 9.0THz. **a–c** Thickness of metallic ring ( $l_1$ ) is 0.02  $\mu\text{m}$ , 0.04  $\mu\text{m}$  and 0.06  $\mu\text{m}$ , respectively. **d–f** Thickness of dielectric layer ( $l_2$ ) is 0.1  $\mu\text{m}$ , 0.2  $\mu\text{m}$ , 0.3  $\mu\text{m}$ , respectively

than the decrements of  $L$ . In conclusion, as the number of metallic rings increases, LC has been increased, the resonant frequency ( $f$ ) will decrease, finally the third absorption peak moves to the left (Fig. 4e).

Figure 8a-c illustrate the electric field distribution of different thickness of metallic ring ( $l_1$ ) at 9.0THz, as  $l_1$  increases the electric field intensity has been decreased, the

**Table 2** Design parameters of proposed absorber

Absorption	BW(THz)	RBW(THz)	Reference
> 80%	1.85–2.48	29%	12
> 80%	1.56–2.24	36%	13
> 80%	1.30–3.00	79%	20
> 80%	2.60–7.80	100%	25
> 80%	2.60–7.80	100%	25
> 80%	0.98–3.53	113%	26
> 80%	1.23–1.68	62%	27
> 80%	2.34–9.98	124%	Our work

absorption at 9.0THz can be decreased (Fig. 4a). When the thickness of  $l_2$  is 7  $\mu\text{m}$ , the electric field intensity of dielectric layer is strongest (Fig. 8e), the absorption at 9.0THz should be highest (green curve Fig. 4b).

Above all, three results can be drawn: 1) the strongest intensity of electric field mainly distributed near the opening structure; 2) the opening structure is response for the absorption peak in NROS absorber, which can also change the distribution of electric field compared to the CNR absorber; 3) the distribution of electric field is symmetrical about the central axis of opening structure. In the proposed structure, the periodic metallic layer is equivalent to an LC (inductance and capacitance) resonance circuit. In this circuit, the intensity of the electric field and the oscillation period (distance between two absorption peaks) are negatively correlated. As a result, the intensity of the electric field of CNR absorber is stronger than that of NROS one [see Fig. 5(g) and Fig. 5(a)], which means the oscillation period of CNR absorber is shorter than that of NROS one. With the reduced oscillation period, the distance between two closed absorption peaks will reduce, thereby the absorption broadband reduces accordingly.

Table 2 summarized our findings with the previous results. Significantly, the proposed NROS absorber shows the largest broadband at high terahertz frequency simultaneously. Bandwidth (BW) and Relative absorption bandwidth (RBW) are two important evaluation indexes of the THz absorber. Compared with the previous results, our designed broadband absorber can cover almost all the high terahertz frequency. This high frequency (equal to short wavelength) absorber can be applied in tiny targets nondestructive detecting and accurate imaging. Meanwhile, the ultra-broadband of 6.04 THz may be used for radar monitoring and terahertz communication.

## 4 Conclusion

In conclusion, we present an ultra-broadband terahertz absorber at high terahertz frequency. The absorption bandwidth is up to 6.04 THz (3.94–9.98 THz) at the absorption above 80%, while a near entire terahertz regime is achieved at the absorption above 60%. Meanwhile, the highest absorption is up to 99.26%, and the average value is still as high as 89.43%. In addition, the proposed absorber exhibits insensitive to the TM and TE polarization no matter what kinds of incident angles are applied. The opening structure is response for such a wide absorption broadband, and the absorption broadband can be regulated by adjusting the incident angle.

**Supplementary Information** The online version contains supplementary material available at <https://doi.org/10.1007/s11082-022-04133-5>.

**Acknowledgements** This work was supported by the National Key R&D Program of China (Grant No. 2019YFA0705201), National Natural Science Foundation of China (Grant No. 61771156), Foundation for Innovative Research Groups of the National Natural Science Foundation of China (Grant No.51521003), Project funded by China Postdoctoral Science Foundation (CA24407217).

**Data availability** The datasets generated during and/or analysed during the current study are available from the corresponding author on reasonable request.

## Declarations

**Conflict of interest** The authors have no relevant financial or non-financial interests to disclose.

## References

- Abramov, I.S., Gospodchikov, E.D., Shalashov, A.G.: Extreme ultraviolet radiation source based on a discharge sustained by a radiation pulse from a terahertz free-electron laser. *J. Exp. Theor. Phys.* **132**(2), 223–232 (2021)
- Bai, J.J., Ge, M.L., Li, J.N., Tang, C.X., Sun, X.D., Xing, H.Y., Chang, S.J.: Numerical investigation of broadband THz metamaterial absorber with double composite structure layer. *Opt. Commun* **423**(15), 63–68 (2018)
- Biabanifard, M., Arsanjani, A., Abrishamian, M.S., Abbott, D.: Tunable terahertz graphene-based absorber design method based on a circuit model approach. *IEEE. Access* **8**(99), 70343–70354 (2020)
- Chen, J.W., Hu, J.D., Deng, X.H., Yuan, J.R.: Enhanced THz absorption of graphene cavity-based electromagnetic metamaterial structures. *J. Mod. Opt.* **67**(6), 547–551 (2020a)
- Chen, X.Z., Liu, X., Guo, X.D., Chen, S., Hu, H., Nikulina, E., Ye, X.L., Yao, Z.H., Bechtel, H.A., Martin, M.C., Carr, G.L., Dai, Q., Zhuang, S.L., Hu, Q., Zhu, Y.M., Hillenbrand, R., Liu, M.K., You, G.J.: THz near-field imaging of extreme subwavelength metal structures. *ACS Photonics* **7**(3), 687–694 (2020b)
- Daraei, O.M., Goudarzi, K., Bemani, M.: A tunable ultra-broadband terahertz absorber based on two layers of graphene ribbons. *Opt. Laser Technol.* **122**, 105853–105857 (2020)
- Feng, H., Xu, Z., Kai, L.I., Wang, M., Yun, M.: Tunable polarization-independent and angle-insensitive broadband terahertz absorber with graphene metamaterials. *Opt. Express.* **29**(5), 7158–7167 (2021)
- Huang, Z., Chen, H., Huang, Y., Ge, Z., Zhou, Y., Yang, Y., Xiao, P.S., Liang, J.J., Zhang, T.F., Shi, Q., Li, G.H., Chen, Y.S.: Ultra-broadband wide-angle terahertz absorption properties of 3D graphene foam. *Adv. Func. Mater.* **28**(2), 1704363–1704371 (2018)
- Huang, J., Li, J., Yang, Y., Li, J., Li, J.H., Zhang, Y., Yao, J.Q.: Active controllable dual broadband terahertz absorber based on hybrid metamaterials with vanadium dioxide. *Opt. Express* **28**(5), 7018–7027 (2020)
- Jiang, Y.N., Zhang, H.D., Wang, J., Gao, C.N., Wang, J., Cao, W.P.: Design and performance of a terahertz absorber based on patterned graphene. *Opt. Lett.* **43**(17), 4296–4299 (2018)
- Landy, N.I., Sajuyigbe, S., Mock, J.J., Smith, D.R., Padilla, W.J.: Perfect metamaterial absorber. *Phys. Rev. Lett.* **100**(20), 207402–207408 (2008)
- Liu, Z., Guo, L., Zhang, Q.: A simple and efficient method for designing broadband terahertz absorber based on singular graphene metasurface. *Nanomaterials* **9**(10), 1351–1355 (2019)
- Lv, J., Yuan, R.Y., Song, X., Yan, H.: Broadband polarization-insensitive terahertz absorber based on heavily doped silicon surface relief structures. *J. Appl. Phys.* **117**(1), 013101–013104 (2015)
- Ma, Y., Chen, Q., Grant, J., Saha, S.C., Khalid, A., Cumming, D.R.S.: Polarisation insensitive, broadband THz metamaterial absorber. *Opt. Lett.* **36**(17), 3476–3478 (2011)
- Mohamadrezza, S., Alireza, N., Iman, C., Sadegh, B.: A configurable two-layer four-bias graphene-based THz absorber. *J. Comput. Electron.* **19**(1), 719–735 (2018)
- Pitchappa, P., Ho, C.P., Cong, L., Singh, R., Singh, N., Lee, C.: Reconfigurable digital metamaterial for dynamic switching offerahertz anisotropy. *Adv. Optical. Mater.* **4**(3), 391–398 (2016)
- Siegel, P.H.: Terahertz technology. *IEEE. Trans. Microw. Theory. Tech.* **50**(3), 910–928 (2002)
- Song, Z., Chen, A., Zhang, J.: Terahertz switching between broadband absorption and narrowband absorption. *Opt. Express* **28**(2), 2037–2044 (2020)

- Song, Z.Y., Wang, K., Li, J.W., Li, Q.H.: Broadband tunable terahertz absorber based on vanadium dioxide metamaterials. *Opt. Express* **26**(6), 7148–7152 (2018)
- Verma, V.K., Mishra, S.K., Kaushal, K.K., Lekshmi, V., Sudhakar, S., Gupta, N., Appasani, B.: An octa-band polarization insensitive terahertz metamaterial absorber using orthogonal elliptical ring resonators. *Plasmonics* **15**(1), 75–81 (2020)
- Wang, B.X., He, Y.H., Wang, N.XXu.X.Y., Wang, Y.C.: Design of dual-band polarization controllable metamaterial absorber at terahertz frequency. *Results. Phys* **17**, 103077–103079 (2020)
- Wang, B.X., Wang, L.L., Wang, G.Z., Huang, W.Q., Li, X.F., Zhai, X.: Theoretical investigation of broadband and wide-angle terahertz metamaterial absorber. *IEEE. Photon. Technol. Lett.* **26**(2), 111–114 (2014)
- Wu, Y.H., Deng, Y.Q., Wang, J.J., Zong, Z.Y., Chen, X., Gu, W.H.: THz broadband absorber fabricated by EHD-printing technology with high error tolerance. *IEEE. Transact. on Terahertz. Sci. Technol.* **9**(6), 637–642 (2019)
- Wu, T., Shao, Y., Ma, S., Wang, G., Gao, Y.: Broadband terahertz absorber with tunable frequency and bandwidth by using dirac semimetal and strontium titanate. *Opt. Express* **29**(5), 7458–7467 (2021)
- Xu, K.D., Li, J., Zhang, A.X., Chen, Q.: Tunable multi-band terahertz absorber using single-layer square graphene ring structure with T-shaped graphene strips. *Opt. Express* **28**(8), 11482–11492 (2020)
- Yen, T.J., Padilla, W.J., Fang, N., Vier, D.C., Smith, D.R., Pendry, J.B., Basov, D.N., Zhang, X.: Terahertz magnetic response from artificial materials. *Science* **303**(5663), 1494–1496 (2004)
- Zhu, D.Y., Wang, Y., Song, L.P., Cui, Z.J.: Semiconductor-based broadband absorber in terahertz band. *Ferrotelectrics* **549**(1), 104–110 (2019)

**Publisher's Note** Springer Nature remains neutral with regard to jurisdictional claims in published maps and institutional affiliations.

Springer Nature or its licensor holds exclusive rights to this article under a publishing agreement with the author(s) or other rightsholder(s); author self-archiving of the accepted manuscript version of this article is solely governed by the terms of such publishing agreement and applicable law.